20th Australasian Fluid Mechanics Conference
Perth, Australia
5-8 December 2016

Bubble formation with a high repetition rate pulsed Tm laser

M. Mohammadzadeh[1], W. Chan[1], S. R. Gonzalez-Avila[1], K. Liu[2], Z. Yan[2], Q. J. Wang[2], and C.D. Ohl[1]

[1]School of Physical and Mathematical Sciences
Nanyang Technological University, Singapore 637371

[2]School of Electrical and Electronic Engineering
Nanyang Technological University, Singapore 639798

Abstract

Thulium lasers are commonly used in medical applications for tissue ablation due to the strong absorption of water in the mid-infrared spectrum. Using high-speed photography, we present an experimental study of bubble formation at the tip of a fiber optic that delivers short pulses of Tm laser at high repetition rates. While a hemispherical bubble forms at the fiber tip at all laser settings, if the power is sufficiently high, a secondary bubble forms during the collapse of the first bubble. The secondary bubble expands at the tip of the initial bubble, moves away from it, and collapses with a jet pointing away from the fiber. A mathematical model is provided to estimate when secondary bubble formation can occur by calculating the maximum bubble radius as a function of the laser power. Finally, the relative translational motion of the bubbles is explained by considering the interaction between two bubbles that oscillate out-of-phase.

Introduction

Mid-infrared (mid-IR) lasers are the standard basis for various laser surgeries, such as fragmentation of urinary stones in laser lithotripsy [17], and removal of arterial blood clots in laser thrombolysis [9]. Mid-IR lasers can efficiently ablate biological tissue by vaporising the water in tissue due to strong absorption of water near the 2 µm wavelength [13]. Additionally, the mid-infrared spectrum can be readily transmitted through standard OH fiber optics. A fundamental part of mid-IR laser surgery is formation of vapor bubbles that act as energy transmission channels, connecting the optical fiber tip to the ablation target [18]. The formation mechanism and dynamics of these bubbles have received attention by researchers to reduce thermal side effects, enhance the ablation efficiency [15], or reduce stone movement in laser lithotripsy [10]. The physical process of formation of these bubbles strongly depends on the laser pulse duration, intensity, and absorption coefficient of the irradiated medium [3, 8].

In the mid-IR spectrum, Thulium (Tm) lasers ($\lambda \approx 1.9$ to 2 µm) are a novel development that offer superior performance compared to common Holmium (Ho) lasers ($\lambda \approx 2$ to 2.1 µm) because of their stronger absorption in water. This allows Tm lasers to increase the tissue ablation efficiency and precision [6]. In the current study, we use a fiber-based Tm laser which produces 1 µs pulses at 1.95 µm wavelength, very close to the 1.94 µm absorption peak of water [16]. The pulses are delivered into water through a fiber of $d = 250$ µm diameter at a high repetition rate, up to 40 kHz. The laser pulse duration τ is longer than stress relaxation time of the liquid, $\tau_{st} = \frac{d}{c}$, where c is the speed of sound. Therefore, strong shock waves are not emitted from the irradiation site. Meanwhile, the pulse duration is shorter than the thermal relaxation time $\tau_{th} = \frac{d^2}{4k}$, k being the thermal diffusivity of the liquid medium. This condition, known as thermal confinement, means that the temperature in the irradiated volume can increase up to the spinodal limit before a vapor bubble forms after phase explosion [5]. Therefore, the vapor bubbles formed with this laser pulse are generated under thermal confinement but not stress confinement, since $\tau_{st} < \tau < \tau_{th}$. These vapor bubbles can generate rapid localized jets which can be utilized for laser tissue ablation; thus, it is essential to investigate the dynamics of these bubbles.

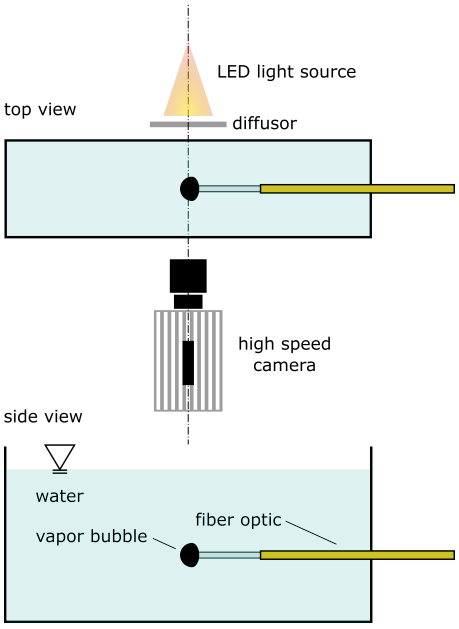

Figure 1: The experimental high-speed photography setup.

In this article, we study the sequential formation of vapor bubbles in water by a Tm laser with high repetition rate. Using high-speed photography, we observe that by increasing the power of the laser at a fixed repetition rate, a new regime of bubble formation occurs, where a secondary bubble expands at the tip of the initial hemispherical bubble. We provide a mathematical model based on an energy balance argument to calculate the maximum bubble radius as a function of the laser energy. This model allows us to determine the laser settings that induce secondary bubble formation. Additionally, we explain the relative translational motion of the two bubbles by considering their out-of-phase oscillation.

Experimental Study

The high-speed photography setup is schematically shown in figure 1. A transparent glass container ($75 \times 45 \times 20$mm) is filled with water, and a fiber optic of diameter $d = 250$ µm is inserted through a small hole in the container. The fiber optic delivers laser pusles from a fiber based Tm laser [16] into water, forming vapor bubbles. The bubble formation and dynamics is observed using a high-speed camera (Photron, FASTCAM SA-X2) with diffused back-illumination from an LED light source

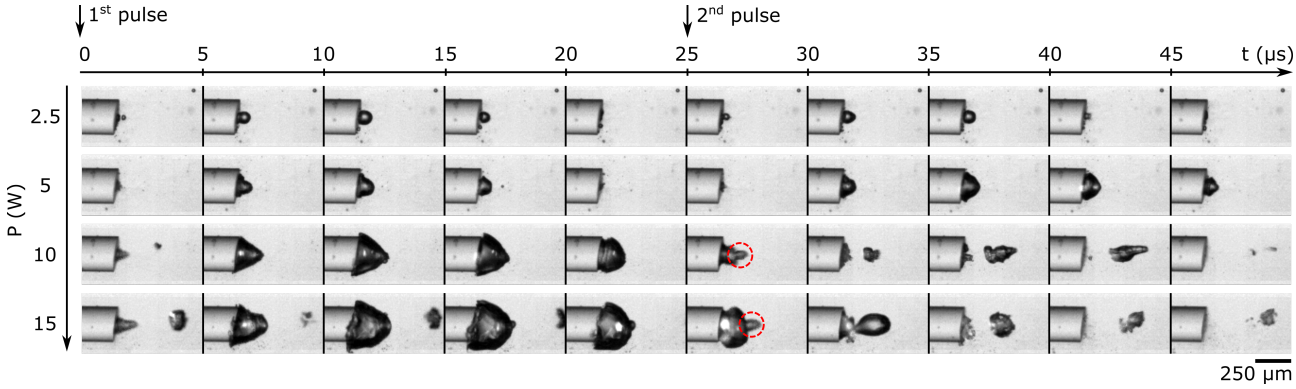

Figure 2: High-speed photography of bubble formation with a pulsed Tm laser at 40 kHz repetition rate. By increasing the average laser power from the top row to the bottom, not only the size of the initial semi-hemispherical bubble increases, but the formation of a secondary bubble can be observed. This occurs when the lifetime of the first bubble is larger than the period of pulse repetition.

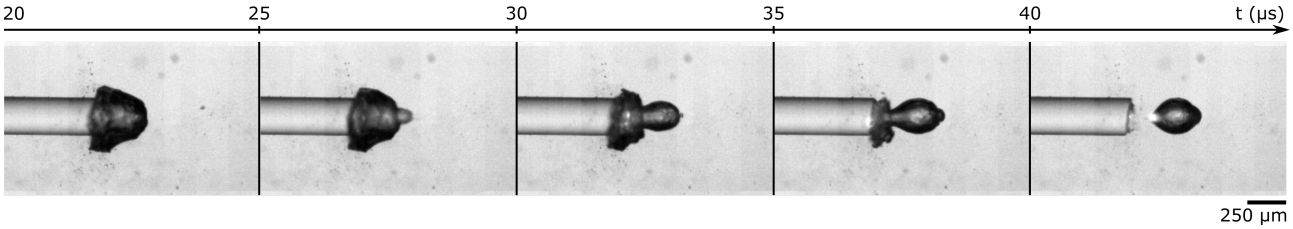

Figure 3: Close-up of secondary bubble formation at 40 kHz and 20 W. At sufficiently high pulse energy, while the first hemispherical bubble is shrinking the next laser pulse arrives, transmitting through the transparent bubble to vaporize the liquid at the distal end of the bubble. While the first bubble collapses back on the fiber tip, the secondary bubble moves away and jets outward.

(REVOX, SLG-150V). Before each set of experiments, the laser pulse duration τ and its repetition rate f are measured with an InGaAs photodiode (Thorlabs, FGA20) connected to an oscilloscope (LeCroy, WaveRunner 64Xi-A). The average power of the laser P is measured with a power meter (Ophir, 30A-BB-18), and the energy of each pulse E is then calculated as $E = P/f$. The experiments are conducted with three different laser repetition rates, $f = 20$, 30, and 40 kHz. The laser power is varied in the range of $P = 2.5$ to 20 W for each repetition rate. For all the laser settings in these experiments, the pulse duration τ is between 800 ns to 1 μs.

Figure 2 shows four series of images of bubble formation and collapse, where the laser power is increased from $P = 2.5$ to 15 W. The repetition rate is fixed at $f = 40$ kHz in this set of experiments, but identical bubble dynamics are observed at other tested repetition rates. As it is shown in the two top rows of figure 2, when the laser power is low, a small, almost hemispherical bubble is formed which collapses at the tip before the next laser pulse. This sequence continues repeatably as long as the laser is on. However, increasing the laser power can drastically affect the bubble shape and dynamics, shown in the bottom two rows of figure 2. If the pulse energy is sufficiently high, the first bubble does not collapse when the next laser pulse arrives. This leads to formation of a secondary bubble at the distal end of the first one. A close-up of the secondary bubble dynamics is shown in figure 3. While the first bubble is shrinking, the secondary bubble expands. Eventually, the first bubble generates a jet toward to the fiber and collapses at the tip surface, but the second bubble moves and collapses away from the tip. While the small fragments of the secondary bubble are still present further away from the fiber, the next laser pulse is absorbed at the liquid layer adjacent to the tip. The cycle repeats with formation of a semi-hemispherical vapor bubble at the tip, similar to the first image in the bottom sequence of figure 2.

Mathematical Model

We can characterize the bubble dynamics observed in the experiments by assuming a hemispherical shape for the initial bubble which grows to a maximum radius of R_{max}. The lifetime of a hemispherical bubble varies linearly with its maximum radius based on the Rayleigh collapse time [2]. Knowing that secondary bubble formation occurs when the lifetime of the bubble is greater than the pulse repetition period, we can link this bubble formation regime to the maximum radius of the initial bubble. In this section, we determine the maximum bubble radius R_{max} as a function of the laser pulse energy E by considering absorption of the laser energy in water and the thermodynamic state of the initial vapor bubble before expansion.

As observed in the experiments, expansion of a bubble formed under thermal confinement occurs very fast compared to the heat conduction time scale τ_{th}. This can be shown by considering that the bubble expansion velocity is greater than the rate of heat transfer [7], resulting in negligible heat loss from the bubble during expansion. Consequently, the bubble undergoes an adiabatic process, $pV^{\gamma} = \text{constant}$, where p is the pressure, V the bubble volume, and γ the adiabatic constant. Based on the simplifying assumption that the bubble remains spherical, we can link the maximum and the initial bubble radius, R_{max} and R_i as

$$(\frac{R_{max}}{R_i})^3 = (\frac{p_i}{p_\infty})^{\frac{1}{\gamma}}. \quad (1)$$

Here p_i is the pressure in the initial vapor bubble before expansion and p_∞ is the ambient pressure exerted on the bubble at its maximum size. To determine the initial bubble radius R_i and pressure p_i, we start from a time when the initial state of the vapor is water at the critical point. Briefly put, this is due to the co-

existence of two distinct phases in the system after vaporization. In the system considered here, the energy deposited from the laser pulse exceeds the vaporization threshold. Although the vaporization process involves non-equilibrium, at some time equilibrium will be established between the two phases. Having two distinct liquid and vapor phases at equilibrium bounds the state of the system to the critical point [4]. The critical pressure, temperature, and density of water are respectively 218 atm, 647 K, and 322 $\mathrm{kg/m^3}$. By fixing the initial state of the system at critical conditions, the initial bubble pressure and density are determined as $p_i = 218$ atm and $\rho_i = 322\,\mathrm{kg/m^3}$. The other unknown remaining in equation 1 is the initial bubble radius R_i, which can be determined by estimating the absorbed energy from the laser pulse, E_{abs}.

The portion of the pulse energy absorbed by the liquid E_{abs} is used to raise the state of the liquid from ambient conditions to the critical point. We denote the energy required to cause this change of state for a specific mass of water as h. Assuming the initial vapor bubble at the tip has a hemispherical shape, the energy balance can be written as

$$\frac{2}{3}\pi R_i^3 \rho_i h = E_{abs}. \tag{2}$$

We can calculate h by following the thermodynamic path in which the temperature of water rises from ambient conditions to 373 K, phase change from liquid to vapor occurs at 373 K, the vapor is heated up under ambient pressure to the critical temperature of 647 K, and finally the steam at critical temperature is pressurized isothermally to the critical pressure of 218 atm. Following the calculation of [7], we find $h = 2.84 \times 10^3\,\mathrm{J/kg}$.

The absorbed pulsed energy E_{abs} can be estimated by considering linear absorption over a hemispherical irradiated volume,

$$E_{abs} = \alpha H_0 V_{irr}. \tag{3}$$

Here α is the linear absorption coefficient of the liquid, H_0 the laser fluence, and V_{irr} the irradiated volume. The absorption coefficient of water at 1.95 µm is approximately $100\,\mathrm{cm^{-1}}$. We calculate the laser fluence by dividing the pulse energy over the fiber tip area uniformly, resulting in $H_0 = E/\pi r_f^2$, where $r_f = d/2$ is the fiber radius. The irradiated volume is modeled as a hemisphere covering the fiber tip $V_{irr} = \frac{2}{3}\pi r_f^3$. By combining these, we find that the absorbed energy is $E_{abs} = \frac{\alpha}{3} E d$. Based on equations 2 and 3, we find that the initial bubble radius is

$$R_i^3 = \frac{\alpha}{2\pi\rho_i h} E d. \tag{4}$$

Having the initial bubble radius, by combining equations 4 and 1 we obtain the maximum bubble radius as a function of the laser energy

$$R_{max}^3 = \left(\frac{p_i}{p_\infty}\right)^{\frac{1}{\gamma}} \frac{\alpha}{2\pi\rho_i h} E d. \tag{5}$$

In figure 4 the maximum bubble radius R_{max} is plotted as a function of the average laser power $P = E f$ for three different repetition rates using equation 5 and compared with the experimental results. The simple model for the bubble radius provides a good quantitative agreement with the experimental results.

We can use this model to determine the laser settings at which secondary bubble formation occurs. The lifetime of a hemispherical bubble can be estimated as twice the Rayleigh collapse time t_c, linked to the maximum bubble radius as $t_c = 0.915\sqrt{\frac{\rho_l}{p_\infty}} R_{max}$, where ρ_l is the density of the liquid surrounding the bubble [2]. For a sufficiently high pulse energy, the first bubble is still present when the next laser pulse arrives. This condition can be quantified as $2t_c > 1/f$. For a fixed pulse repetition rate f, the laser power $P = Ef$ needed for transition to secondary bubble formation can be calculated from equation 5 by setting $R_{max} = \frac{1}{2\times 0.915 f}\sqrt{\frac{p_\infty}{\rho_l}}$. This laser power is plotted as a function of the repetition rate f in figure 5, which is in good agreement with the bubble formation regime observed experimentally.

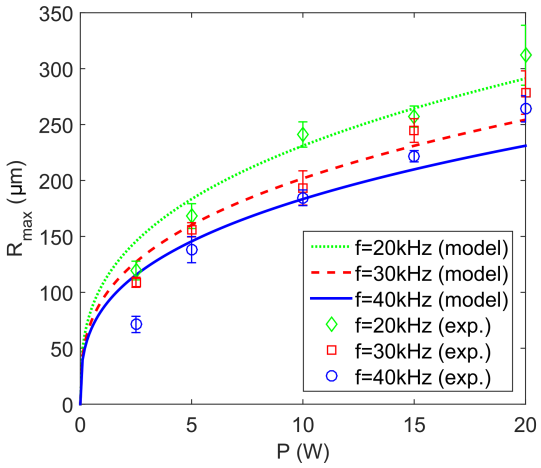

Figure 4: Maximum bubble radius R_{max} as a function of the average laser power P. The experimental results are compared with the model presented in equation 5 for three different laser repetition rates.

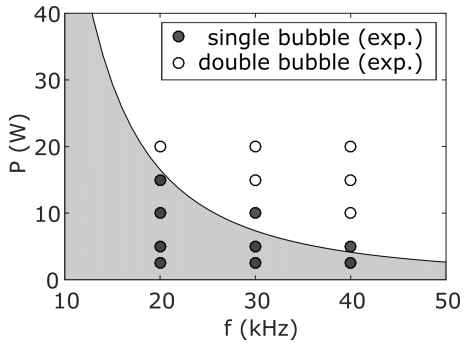

Figure 5: Laser power P needed for secondary bubble formation as a function of the pulse repetition rate f. The gray color marks the region and experimental data (circles) with only hemispherical bubble formation, and white denotes the formation of secondary bubbles.

Interaction Between the Bubbles

In the experiments we observe an interaction between the dynamics of the two bubbles during secondary bubble formation: while the first bubble shrinks the second expands, and their distance increases over time. This relative motion is particularly interesting, because the secondary bubble does not collapse on the tip surface as the first one does; instead, the secondary bubble jets outward and collapses away from the tip. This seems

counter-intuitive, considering that cavitation bubbles tend to jet toward solid boundaries and collapse at the surface [11]. Nevertheless, the relative motion of these bubbles can be explained by considering the out-of-phase oscillations of two bubbles.

It is known that two spherical bubbles either attract or repel each other, based on whether their oscillations are in-phase or out-of-phase [1, 14, 19]. In this case, we observe a similar behavior between a semi-hemispherical bubble forming at the tip and a semi-spherical bubble that expands further away. In our experiments, the expansion of the second bubble starts during the shrinkage of the first; therefore, their oscillations are out-of-phase. Similar to the case of two spherical bubbles, the two bubbles in the experiments repel each other and the second bubble collapses when it is further away from the tip.

Discussion and Conclusion

Mid-infrared lasers play a major role in laser surgeries due to their strong absorption by the water contents of biological tissue. Long mid-IR pulses, in the order of a few hundred microseconds, can generate elongated, pear shaped bubbles, such as those created in Ho:YAG laser lithotripsy [5]. By combining different mid-infrared lasers, the bubble shape can be modified and utilized to enhance tissue ablation [15]. Additionally, the dynamics of these bubble are linked to challenges such as stone movement in laser lithotripsy. It has been proposed to change the bubble shape to mitigate stone retropulsion in this procedure by modifying the temporal pulse profile [12].

Contrary to long pulse durations, for short pulses of the order of 1 µs, pear shaped bubbles have not been observed and the bubbles are almost hemispherical. In this work, we find that bubbles generated by short pulses at sufficiently high repetition rates can also have non-spherical shapes, such as those shown in figure 3. This may be applied for formation a of vapor channel through the absorbing medium with quick sequences of short pulses. The simple model provided can be used to determine the bubble size as a function of the laser energy in good quantitative agreement with the experiments, and determine the laser settings leading to secondary bubble formation. Interaction of the two bubble and the resulting rapid liquid jets may be useful for tissue ablation.

References

[1] Bjerknes, V., Fields of force.

[2] Brennen, C., *Cavitation and bubble dynamics*, Cambridge University Press, 2013.

[3] Brinkmann, R., Hansen, C., Mohrenstecher, D., Scheu, M. and Birngruber, R., Analysis of cavitation dynamics during pulsed laser tissue ablation by optical on-line monitoring, *IEEE J. Sel. Top. Quant.*, **2**, 1996, 826–835.

[4] Cleary, S., Laser pulses and the generation of acoustic transients in biological material, in *Laser applications in medicine and biology*, Springer, 1977, 175–219.

[5] Frenz, M., Könz, F., Pratisto, H., Weber, H., Silenok, A. and Konov, V., Starting mechanisms and dynamics of bubble formation induced by a ho: Yttrium aluminum garnet laser in water, *J Appl. Phys.*, **84**, 1998, 5905–5912.

[6] Fried, N. and Murray, K., High-power thulium fiber laser ablation of urinary tissues at 1.94 um, *J. Endourol.*, **19**, 2005, 25–31.

[7] Gerstman, B., Thompson, C., Jacques, S. and Rogers, M., Laser-induced bubble formation in the retina, in *Photonics West'95*, International Society for Optics and Photonics, 1995, 60–71, 60–71.

[8] Jansen, E., Asshauer, T., Frenz, M., Motamedi, M., Delacretaz, G. and Welch, A., Effect of pulse duration on bubble formation and laser-induced pressure waves during holmium laser ablation, *Laser. Surg. Med.*, **18**, 1996, 278–293.

[9] Jean, B. and Bende, T., Mid-ir laser applications in medicine, in *Solid-State Mid-Infrared Laser Sources*, Springer, 2003, 530–565.

[10] Kang, H. W., Lee, H., Teichman, J., Oh, J., Kim, J. and Welch, A., Dependence of calculus retropulsion on pulse duration during ho: Yag laser lithotripsy, *Laser. Surg. Med.*, **38**, 2006, 762–772.

[11] Lauterborn, W. and Bolle, H., Experimental investigations of cavitation-bubble collapse in the neighbourhood of a solid boundary, *J. Fluid Mech.*, **72**, 1975, 391–399.

[12] Mohammadzadeh, M., Mercado, J. and Ohl, C., Bubble dynamics in laser lithotripsy, in *J. Phys. Conf. Ser.*, IOP Publishing, 2015, volume 656, 012004, 012004.

[13] Palmer, K. and Williams, D., Optical properties of water in the near infrared, *J. Opt. Soc. Am.*, **64**, 1974, 1107–1110.

[14] Pelekasis, N. and Tsamopoulos, J., Bjerknes forces between two bubbles. part 1. response to a step change in pressure, *J. Fluid Mech.*, **254**, 1993, 467–499.

[15] Pratisto, H., Frenz, M., Ith, M., Altermatt, H., Jansen, E. and Weber, H., Combination of fiber-guided pulsed erbium and holmium laser radiation for tissue ablation under water, *Appl. Optics*, **35**, 1996, 3328–3337.

[16] Tang, Y., Li, X., Yan, Z., Yu, X., Zhang, Y. and Wang, Q., 50-w 2-μm nanosecond all-fiber-based thulium-doped fiber amplifier, *IEEE J. Sel. Top. Quant.*, **20**, 2014, 537–543.

[17] Vassar, G., Chan, K., Teichman, J., Glickman, R., Weintraub, S., Pfefer, T. and Welch, A., Holmium: Yag lithotripsy: photothermal mechanism, *J. Endourol.*, **13**, 1999, 181–190.

[18] Vogel, A. and Venugopalan, V., Mechanisms of pulsed laser ablation of biological tissues, *Chem. Rev.*, **103**, 2003, 577–644.

[19] Yuan, F., Sankin, G. and Zhong, P., Dynamics of tandem bubble interaction in a microfluidic channel, *J. Acoust. Soc. Am.*, **130**, 2011, 3339–3346.